Optical-data model for the stopping power of condensed matter for protons and antiprotons

1991 J. Phys.: Condens. Matter 3 2741

(http://iopscience.iop.org/0953-8984/3/16/014)

J. Phys.: Condens. Matter 3 (1991) 2741–2753. Printed in the UK

Optical-data model for the stopping power of condensed matter for protons and antiprotons

J C Ashley
Health and Safety Research Division, Oak Ridge National Laboratory, Oak Ridge, Tennessee 37831-6123, USA

Received 6 August 1990, in final form 14 November 1990

Abstract. A model for the energy-loss function of a medium that is based on optical data (~zero momentum transfer) and a quadratic extension into the momentum-transfer plane is used to evaluate the stopping power of the medium for protons and antiprotons. Energies less than ~40 MeV are considered for which radiative energy losses and density-effect corrections are negligible. 'Higher-order' corrections to the stopping power proportional to the incident particle charge to the third power, Barkas effect, and to the fourth power, Bloch correction, are included. Calculations are presented for aluminum, carbon, copper and polystyrene. Comparisons with experimental data indicate that the optical-data model, plus higher-order corrections, provides an excellent description of energy loss for proton energies from ~100 keV to several tens of MeV.

1. Introduction

The rate of energy loss by charged particles traversing matter, that is the stopping power of matter for charged particles, is a subject of longstanding experimental and theoretical interest. Theoretical descriptions for heavy particles usually appeal to the Bethe theory of stopping power as outlined in [1] and [2]. Predictions from this theory for non-relativistic particles require a material-dependent parameter, the mean excitation energy, which is usually extracted from experimental stopping-power data, and shell corrections supplied by supplementary theoretical calculations. If the response of the given medium was known for all possible energy and momentum transfers (or the generalized oscillator strength), the stopping power could be calculated without the need for additional information. Since this comprehensive information is not available, models based on optical data (zero momentum transfer) for the medium and reasonable assumptions about the response to momentum transfers can be used as approximations for evaluating stopping power. One such model is employed in this paper to obtain the stopping powers of several solids. The advantage of this procedure, as discussed in detail below, is that the mean excitation energy need not be known explicitly and the shell corrections are 'built into' the model.

The 'optical-data' model introduced previously [3, 4] for predicting electron and positron energy loss and inelastic mean free path is applied to calculate the stopping power of matter for protons and antiprotons. The basis of the model is an expression for the energy-loss function which assumes a simple quadratic dependence on momentum

0953-8984/91/162741 + 13 $03.50

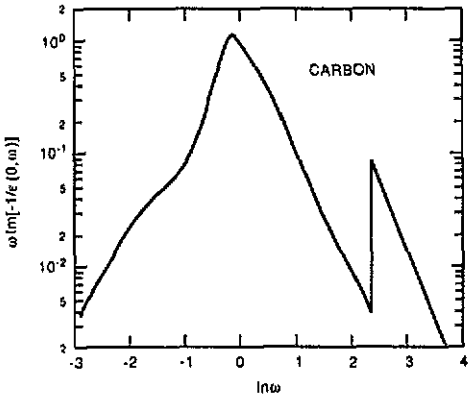

Figure 1. Shape of the GOS in the $q = 0$ limit (optical oscillator strength) based on optical data for carbon.

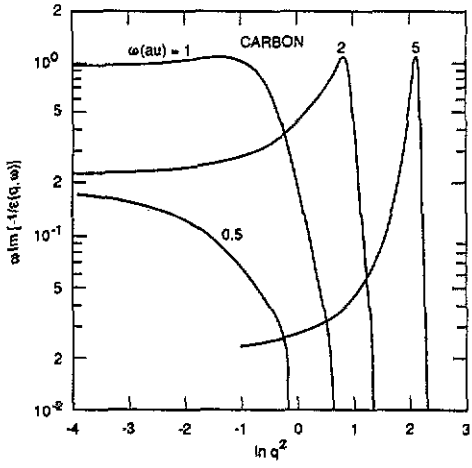

Figure 2. Behaviour of the optical-data model GOS as a function of momentum transfer for small energy transfers.

transfer q. For simplicity, we work in the system of atomic units where $\hbar = e = m = 1$. More widely recognized, conventional units will be used to describe results. For an energy transfer ω, the energy-loss function, or dielectric response function, $\mathrm{Im}[-1/\varepsilon(q, \omega)]$, is connected with the optical energy-loss function ($q = 0$), and hence experimental optical data, through

$$\omega\,\mathrm{Im}[-1/\varepsilon(q,\omega)] = \int_0^\infty \mathrm{d}\omega'\,\omega'\,\mathrm{Im}[-1/\varepsilon(0,\omega')]\delta[\omega - (\omega' + q^2/2)]. \tag{1}$$

Note that $\omega\,\mathrm{Im}[-1/\varepsilon(q, \omega)]$ is proportional to the generalized oscillator strength (GOS) for the medium. A general review of the GOS and its importance has been provided by Inokuti and co-workers [1, 2]. The energy-loss sum rule, or the oscillator-strength sum rule, is

$$\int_0^\infty \mathrm{d}\omega\,\omega\,\mathrm{Im}[-1/\varepsilon(q,\omega)] = \frac{\pi}{2}\Omega_\mathrm{p}^2 \tag{2}$$

where $\Omega_\mathrm{p}^2 \equiv 4\pi n_0 Z_2$, and n_0 is the density of atoms or molecules in the medium with Z_2 electrons per atom or molecule. This sum rule is obeyed for all q if the input optical data $\mathrm{Im}[-1/\varepsilon(0, \omega)]$ obey equation (2).

For comparison with GOSs from atomic models discussed in [1], we illustrate the form of equation (1) using optical data on carbon [5]. Figure 1 gives ω times the optical energy loss function for carbon based on the data in [5]. The main features in this figure are a broad maximum at $\omega \approx 0.86$ (or $\hbar\omega \approx 23$ eV) and the onset of K-shell ionization at $\omega \approx 10.4$ ($\hbar\omega \approx 282$ eV). Obviously this information will be reproduced by equation (1) in the limit $q \to 0$. Figures 2 and 3 show the shape of the GOS predicted from equation 1 as a function of momentum transfer for several values of energy transfer. These figures show the emergence of the 'Bethe ridge', i.e., the concentration of the GOS around the line $\omega = q^2/2$, for large q and ω. For large enough energy transfer, K-shell ionization begins to contribute to the GOS as shown in figure 3. The GOS approximated by equation (1) thus has the expected limiting form for $q \to 0$ as well as for large q and ω, and, as

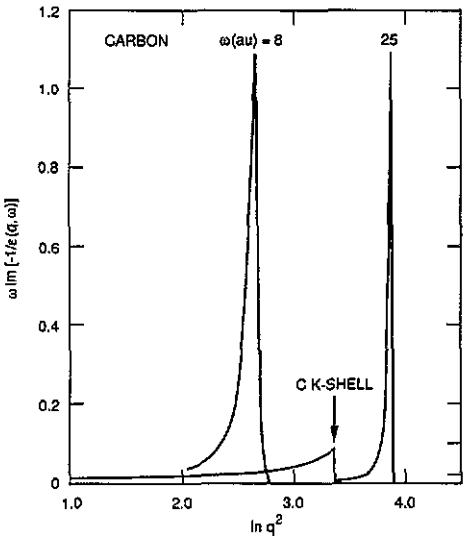

Figure 3. Behaviour of the optical-data model GOS as a function of momentum transfer for large energy transfers. The K-shell contribution is seen as a small feature on the $\omega = 25$ curve.

importantly since stopping power is evaluated by integration over the GOS, obeys the sum-rule constraint of equation (2) for any value of q.

In this paper we start by describing the lowest-order (proportional to the square of the incident-particle charge) contribution to the stopping power of the medium using the *ansatz* for the GOS described by equation (1). Our emphasis is on energies up to several tens of MeV so that radiative energy losses and density-effect corrections are negligible. 'Higher-order' corrections, proportional to the third and fourth powers of the incident particle charge, are important for these energies and will be incorporated. These results can be related to the usual Bethe theory of stopping power as reviewed in [1], [2] and [6]. Results for the stopping powers for aluminum, carbon, copper and polystyrene will be presented and comparisons made with experimental data.

2. The optical-data model stopping power

The stopping power of a medium described by the energy-loss function $\mathrm{Im}[-1/\varepsilon(q,\omega)]$ for a proton ($Z_1 = 1$) or antiproton ($Z_1 = -1$) of speed v is given by [7, 8]

$$S(v^2) = \frac{2Z_1^2}{\pi v^2}\int \mathrm{d}\omega\,\omega \int \frac{\mathrm{d}q}{q}\,\mathrm{Im}[-1/\varepsilon(q,\omega)]. \tag{3}$$

The limits on the q integration are $\omega/v \leqslant q < \infty$; and ω varies from zero to $\omega = 2v^2$, the maximum energy transfer to a free electron in the medium. Equations (1) and (3) give

$$S(v^2) = \frac{2Z_1^2}{\pi v^2}\int_0^{v^2/2} \mathrm{d}\omega'\,\omega'\,\mathrm{Im}[-1/\varepsilon(0,\omega')]H(\omega'/v^2) \tag{4}$$

where

$$H(a) \equiv \ln[(1 - a + s)/a] \tag{5}$$

and $s = (1 - 2a)^{1/2}$. In the high-speed, but non-relativistic, limit we obtain the usual Bethe-theory result for $Z_1 = \pm 1$:

$$S(v^2) \approx (\Omega_p^2/v^2)\ln(2v^2/I) \tag{6}$$

where I is the mean excitation energy defined by

$$\ln I \equiv \frac{2}{\pi\Omega_p^2}\int_0^\infty d\omega'\,\omega' \ln\omega' \operatorname{Im}[-1/\varepsilon(0,\omega')]. \tag{7}$$

An important feature of the expression for S in equation (4) is that as one goes to lower values of v, and thus lower values of maximum energy transfer, the reduction and eventual elimination of inner-shell contributions to the stopping process is incorporated automatically. That is, 'shell corrections', which must be provided by separate calculations in the usual Bethe-theory approach, are incorporated in the expression for S. In the standard notation, shell corrections may be extracted through [9]

$$C/Z_2 \equiv \ln(2v^2/I) - L_0 \tag{8}$$

where

$$L_0 \equiv v^2 S(v^2)/\Omega_p^2 Z_1^2. \tag{9}$$

Shell corrections determined in this manner will be compared with other results in Section 4.

3. Higher-order corrections

To the basic stopping power expression, equation (4), we add corrections of higher power, namely, the Barkas-effect correction, proportional to Z_1^3 [10], and the Bloch correction [6, 11], proportional to Z_1^4. The total stopping power is written as

$$S = (Z_1^2\Omega_p^2/v^2)(L_0 + Z_1 L_1 + L_2) \tag{10}$$

where L_0 is to be evaluated from the optical-data model through equation (9), L_1 is the Barkas-effect correction, and L_2 is the Bloch correction. These correction terms are discussed extensively elsewhere, as reviewed in [6], e.g.; we present the terms in a form suitable for numerical evaluation.

For $y^2 = Z_1^2/v^2 < 1$, L_2 is approximated very closely by [12]

$$L_2 = -y^2[1.20206 - y^2(1.042 - 0.8549y^2 + 0.343y^4)]. \tag{11}$$

To obtain L_1, start with [10]

$$L_1(\omega) = (\omega/v^3)I(\xi) \tag{12}$$

where $\xi \equiv a\omega/v$, with a a minimum impact parameter to be discussed later, and $I(\xi)$ is a tabulated function [13]. For easy numerical calculation this function may be approximated by:

$$I(\xi) = \begin{cases} (3\pi/2)\ln(1/\xi) - 2.417 - 2\pi\xi^2[(\ln\xi)^2 + 1.14\ln\xi - 0.33] & \xi < 0.25 \\ (-0.5986 + 0.9962/\xi - 0.1233/\xi^2)\xi^{-3/4} & 0.25 \leqslant \xi < 1 \\ 9.052\exp(-3.72\xi + 0.217\xi^2) & 1 \leqslant \xi \leqslant 2. \end{cases}$$

The analytic form for small ξ was derived in [14] and reproduces tabulated values to within 1% for $\xi \leqslant 0.2$ increasing to 1.7% at $\xi = 0.25$. The other terms were found

by fitting the tabulated values—to within 2% for $0.25 \leqslant \xi < 1$ and within 0.2% for $1 \leqslant \xi \leqslant 2$.

Equation (12) represents a 'distant-collision' (small q) contribution to stopping power so we take a distribution of ωs determined by the optical energy-loss function through

$$G(\omega) = \omega \operatorname{Im}[-1/\varepsilon(0, \omega)] \left\{ \int_0^\infty \mathrm{d}\omega\, \omega \operatorname{Im}[-1/\varepsilon(0, \omega)] \right\}^{-1}. \tag{14}$$

Thus

$$L_1 = \int_0^{\omega_{\max}} \mathrm{d}\omega\, G(\omega) L_1(\omega) \tag{15}$$

with $\omega_{\max} = 2v^2$. In [10] a statistical model for $G(\omega)$ was used for the target atoms leading to

$$L_1 = F(b/x^{1/2})/Z_2^{1/2} x^{3/2} \tag{16}$$

where $x \equiv v^2/Z_2$, $b = \eta\chi Z_2^{1/6}$ with η a parameter of order 1, and χ a constant from the statistical model; F is a tabulated function [13]. In practice, in relating Bethe theory plus correction terms to careful experimental stopping power measurements, b and χ are taken as fitting parameters (see, e.g., [15–17] and references therein). An example of this usage will be discussed in the next section.

4. Calculations and comparisons

In this section we present the results for stopping power, and related quantities, for protons in several materials. Comparisons will be made with experimental data and other theoretical results. Aluminum will be emphasized as a test case for the model.

4.1. Aluminum

Aluminum is considered first because of the existence of excellent stopping power data [16, 17] and optical data. A carefully tested, composite set of optical data for Al is available up to $\hbar\omega = 10^4$ eV [18, 19]. For higher photon energies we take $\operatorname{Im}[-1/\varepsilon(0, \omega)] \propto \omega^{-4}$. The set of data included in the program to calculate S yields from the sum rule, equation (2), a value of Ω_p^2 which is 0.1% less than the expected value 1.4569 and a value of $\ln I(\mathrm{eV}) = 5.0948$ [$\Rightarrow I(\mathrm{eV}) = 163.2$] which is ~0.3% less than ln(165.7) given in [18].

For the stopping power calculations we relate the proton's speed to its kinetic energy E through $v^2 = c^2[1 - (1 + E/Mc^2)^{-2}]$, where M is the proton mass, or non-relativistically $v^2\,(\mathrm{au}) = E\,(\mathrm{keV})/25$. Two choices for the minimum impact parameter a were used to calculate L_1: (*i*) $a = 1/\sqrt{2\omega}$ suggested by Jackson and McCarthy [20], and (ii) $a = 1/1.781v$ as suggested by Lindhard [21].

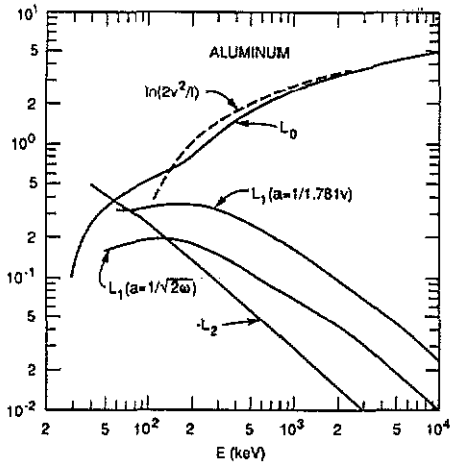

Figure 4. Comparison of L_0 for aluminum with the 'Bethe-logarithm' term. Barkas-effect corrections L_1 are shown for two choices of minimum impact parameter a; L_2 is the Bloch correction.

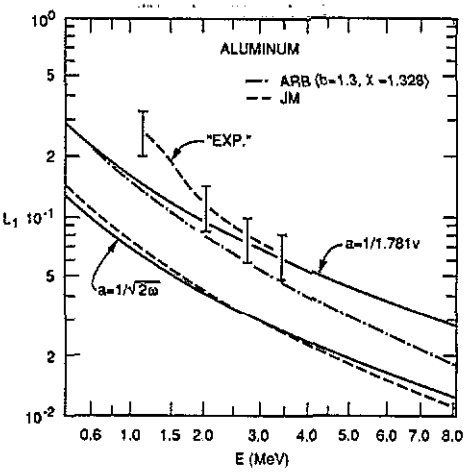

Figure 5. Comparison of L_1 evaluated from optical data with statistical model results and with experimental results. Details in text.

The calculations for Al are summarized in figure 4 as functions of proton energy. L_0, determined from equations (4), (5) and (9) with the optical data for aluminum, is compared with the simple, high-speed result $\ln(2v^2/I)$. The predictions for L_1 differ by a factor of ~1.5–2 over the energy range shown as expected from earlier discussions [21]. The Bloch term is negative and is displayed as $-L_2$ in the figure. At the lower energies, ≤ 100 keV, the 'correction' terms begin to dominate the behaviour of the stopping power and the validity of this approach becomes questionable.

L_1 is shown in more detail in figure 5 where the experimental value determined from stopping power data (broken curve with error bars) [22] is included. The L_1s calculated with the optical data are indicated by the choice of a. The curve labelled 'ARB' was determined from equation (16) using parameter values fixed by fits to stopping power data [23]. The curve 'JM' is from [20] where $a = 1/\sqrt{2\omega}$ was taken and a statistical model used to arrive at an essentially parameter-free form of equation (16). This result agrees quite well with our optical-data result using the same choice for a. Since our calculated L_1 with $a = 1/1.781v$ agrees reasonably well with the experimental results and with L_1 from fits to experimental stopping-power data, particularly at the lower energies where it contributes more significantly to the total stopping power, we will adopt this value of a for calculations on other materials.

A direct measure of the Barkas-effect correction is found by measuring the difference in energy between a proton (p) and an antiproton ($\bar{p}$), with the same initial energies, after transmission through a given thickness of material t. This energy difference $\Delta E \equiv E_{\bar{p}} - E_p$ is proportional to $2L_1 t$ for small t. Recent experiments give $\Delta E = 194 \pm 45$ keV for 5.9 MeV particles after 117 μm of aluminum plus 107 μm of 'aluminum equivalent' material (Ti, plastics, and gases) [24].

In figure 6 are shown the energy of a proton, with initial energy 5.9 MeV, as a function of path length in Al; ΔE is calculated with $a = 1/1.781v$, and with L_1 from equation (16) for $b = 1.3, \chi = 1.328$ [23]. The experimental result [24], ΔE (keV) = 194 ± 45, appears consistent with either method for calculating L_1 assuming all 224 μm of the material *is*

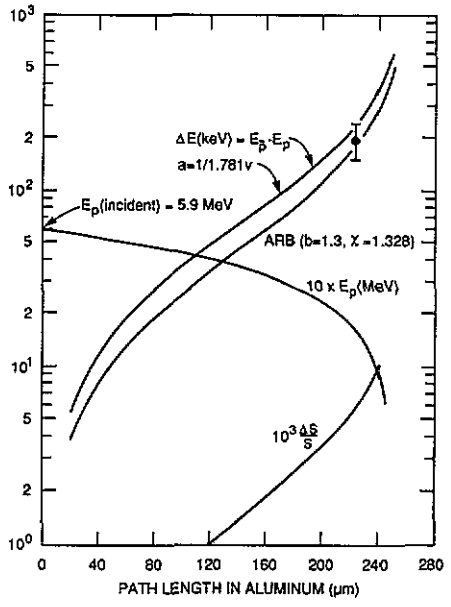

Figure 6. Proton energy, and antiproton–proton energy difference ΔE as functions of path length in aluminum. ΔE was calculated for two forms for L_1. Experimental point from [24]. Deviation of path length from penetration depth is given by $\Delta s/s$.

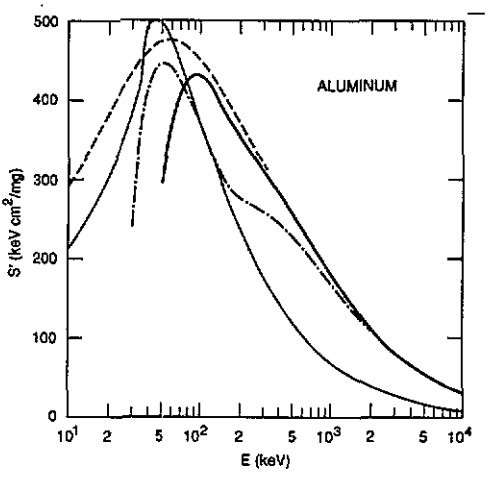

Figure 7. Comparison of stopping power of aluminum for protons calculated from the optical-data model (heavy, full curve) with a fit to collected experimental data (broken curve). The light, full curve is from an electron-gas model (for conduction electrons only); the chain curve is from the optical-data model without higher-order corrections.

aluminum. The difference in the calculated ΔEs at this pathlength is ~30%. The choice $a = 1/\sqrt{2\omega}$ gives $\Delta E = 102$ keV for 224 μm of aluminum, well below the experimental result. We note that measurements of ΔE, and hence L_1, in thin films of silicon are available for energies from 500 keV to 3 MeV [25].

As a measure of the deviation of the pathlength s travelled by a proton, from the depth of penetration (or target thickness) due to multiple scattering, the quantity [9]

$$\Delta s \equiv \langle s - t \rangle_s = \int_0^s \langle 1 - \cos\theta \rangle_{s'} \, ds' \tag{17}$$

was calculated using a simple theory of multiple scattering [26] for a proton of initial energy 5.9 MeV in aluminum. Shown in figure 6 as $\Delta s/s$, the multiple scattering calculations indicate a correction <1% and thus do not influence the theory–experiment comparison. For small path lengths, $\Delta s/s$ is approximately the same as $\langle\theta^2\rangle/4$ used for path length corrections in thin foils [17]; for $s = 160$ μm, $\langle\theta^2\rangle/4$ underestimates $\Delta s/s$ by about a factor of two.

The mass stopping power, $S' = S/\rho$, of aluminum, calculated with the optical data model plus the $L_1(a = 1/1.781v)$ and L_2 correction terms, is shown as the heavy full curve in figure 7. The change in the slope of this curve in the region 150–200 keV is due to the onset of contributions to the stopping from L-shell electrons. The broken curve represents a fit to a large amount of experimental data as reported in [27]. Agreement

Table 1. Stopping power of aluminum for protons (in keV cm^2 mg^{-1}).

E (MeV)	This work	Aarhus [22]	Nara† [16]	Risö [28]
0.8	201.5	196.6		
1	176.7	172.1		
1.2	157.6	153.6		
1.4	142.5	139.0		
1.6	130.2	127.3		
1.8	120.0	117.6		
2	111.4	109.5		
3	82.98	82.39	82.26	83.23
4	67.51	66.96	67.00	67.72
5	57.40	56.88	56.94	57.57
6	50.16	49.70	49.74	50.28
7	44.69		44.31	44.76
8	40.39		40.05	40.44
9	36.91		36.60	36.96
10	34.04		(33.76)	34.09
12	29.55		(29.32)	29.60
14	26.20		(26.01)	26.26
16	23.60		(23.43)	23.67
18	21.51		(21.37)	21.59

† Table 5, 'smoothed data'

for $E > 100$ keV is quite good overall; the curves differ by 4–6% up to ~300 keV, within 2% up to 4000 keV, and then ~4% at 10 MeV. At the lower energies the differences are considerably smaller than the spread in the data sets shown in [27]. For energies less than or equal to 100 keV the sizes of the correction terms become comparable with L_0 (see figure 4) so this calculation is not expected to be meaningful at low energies.

The chain curve in figure 7 is S' calculated using L_0 only (no higher-order corrections). Comparison with the heavy, full curve illustrates the increasingly important role of the higher-order terms at lower energies. The light full curve is S' calculated using an electron-gas model [7] to describe the conduction electrons (only) in aluminum. The peak of this curve and the L_0-only result (chain curve) occur at about the same energy and differ by ~15% at the peaks. These curves come together on the high-energy side of the peak, but separate at higher energies as the L-shell electrons begin to contribute to the optical-model calculation at ~140 keV.

A more detailed comparison can be made with careful measurements (stated errors of ~1/2%) collected in table 1 from [16] ('Nara'), [22] ('Aarhus'), and [28] ('Risö'). As discussed in [16], the differences in the Nara and Aarhus data are within the statistical uncertainty in the overlapping energy region while the Risö data are greater than the Nara data by ~1%. Our calculations fall in between the latter two sets for $E \geq 3$ MeV, being from ~0.7 to 0.9% greater than the Nara data and from ~0.2 to 0.4% less than the Risö values. Differences of ~2–3% between model calculations and data are found at energies <3 MeV. These comparisons indicate the validity and usefulness of this model for predicting stopping powers of materials for which optical data are avalable over a wide range of photon energies.

As mentioned earlier, evaluation of L_0 from the optical data automatically includes the 'shell corrections'. These are evaluated from equation (8) and shown by the full line

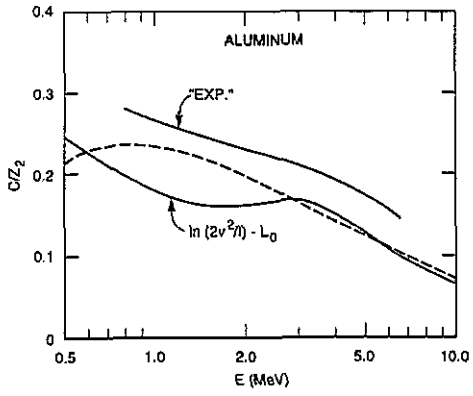

Figure 8. Comparison of the shell-correction term extracted from the optical-data model with the Bonderup statistical model result (broken curve) and with that determined from experimental data.

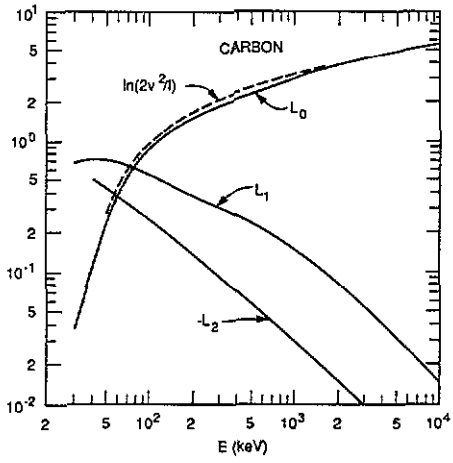

Figure 9. Comparison of L_0 for carbon with the 'Bethe-logarithm' term. L_1 is the Barkas-effect correction and L_2 the Bloch correction.

in figure 8. The bump at ~3 MeV is due to the K-shell in Al which does not contribute to stopping for $E < 2.8$ MeV. The full line marked 'EXP' was determined from stopping-power data [22] and the broken curve is from Bonderup's theoretical model [29]. In the context of shell-correction studies, the agreement shown in this figure should be considered to be quite good.

4.2. Carbon

The optical data for arc-evaporated carbon films [5] were used to calculate stopping power using the optical-data model plus correction terms as outlined above. The sum rule for the data in the program gave a value of Ω_p^2 about 1/3% larger than the predicted value 1.0631. If values of the optical energy-loss function are reduced by 1% above the K edge ($\hbar\omega = 282$ eV), exact agreement is obtained for the sum rule, and the mean excitation energy is $I = 82.6$ eV. The results are shown in figure 9 with $a = 1/1.781v$ in L_1 and $\ln(2v^2/I)$, broken curve, for comparison with L_0. The total mass stopping power is shown in figure 10 with the fitted curve (broken curve) from [27]. These two curves agree to within ~1% for $E > 1$ MeV; differences increase to ~15% near the peak at 80 keV. The chain curve is calculated with L_0 only and illustrates, once more, the strong influence of the higher-order corrections at the lower energies. In figure 11 we compare the model shell corrections for C and Al with the semi-empirical shell corrections suggested in [30].

4.3. Polystyrene

Optical properties of polystyrene over a large range of photon energies [31] have been employed to evaluate stopping powers. The optical data yield excellent agreement for the sum rule and a value of $I = 68.5$ eV which differs insignificantly from the value predicted earlier using essentially the same optical data [32].

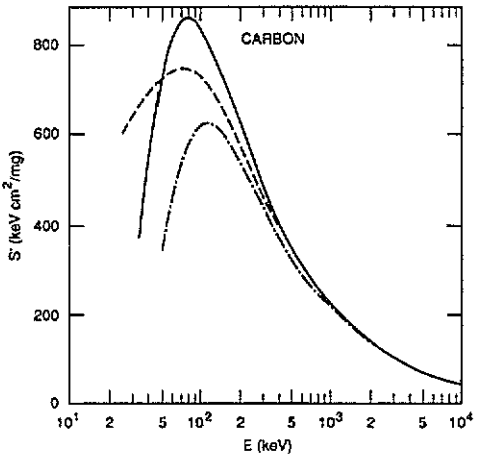

Figure 10. Stopping power of carbon for protons (full curve) with a fit to collected experimental data. The chain curve includes L_0 only.

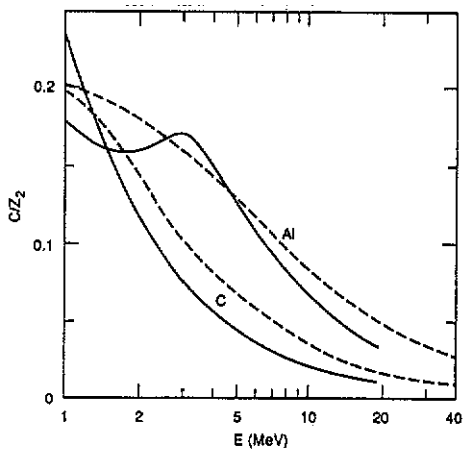

Figure 11. Shell corrections for carbon and aluminum from the optical-data model (full curves) compared with the recommended values [30].

The mass stopping power of polystyrene for protons calculated from the optical-data model plus higher-order corrections is given by the full curve in figure 12. The higher-order correction terms account for ~25% of the total stopping power at 100 keV and ~40% at 60 keV. For comparison, the broken curve is from a tabulation [33] based, to some extent, on experimental data. Our results are ~20% larger in the peak region, cross at ~250 keV, and are approximately less than 2% less than those tabulated values for $E > 300$ keV. Most of the differences at the higher energies can be accounted for by differences in the I values (61.4 eV for the tables and 68.5 eV for the optical-data model) through $\Delta S'/S' \approx [\ln(68.5/61.4)]/\ln(2v^2/I) \sim 0.02$ at 10 MeV.

Measurements of mass stopping of polystyrene for protons are available for $2\,\text{MeV} < E < 6\,\text{MeV}$ [34, 35]. The inset in figure 12 gives the ratios of the calculated values to the experimental data accounting for the uncertainties in the data. Excluding the value at 4351 keV, the model seems to predict values ~1% greater than the experimental data over this energy range; this is consistent with the difference between $I = 71.1 \pm 1.8$ eV derived from the measured energy loss, and the value of I determined from the optical data.

In figure 13 we compare the shell-correction terms extracted from the optical-data model, equation (8), for carbon and polystyrene. The differences here reflect the different distributions of optical oscillator strength, defined by equation (14), for these two materials. For carbon, half the optical oscillator strength lies below 47 eV, while for polystyrene the optical oscillator strength is more concentrated at lower energies, with half the strength below 36 eV.

4.4. Copper

Optical data for several materials are compiled in a DESY report [36]. These data have not been subjected to the rigorous re-analysis applied to those for aluminum [18]. The data for copper from these tables, plus extension to higher energies assuming $\text{Im}[-1/\varepsilon(0, \omega)] \propto \omega^{-4}$, give a sum-rule value for $\pi\Omega_p^2/2$ about 2% too small and $I = 312$ eV, somewhat lower than generally accepted values [16, 30].

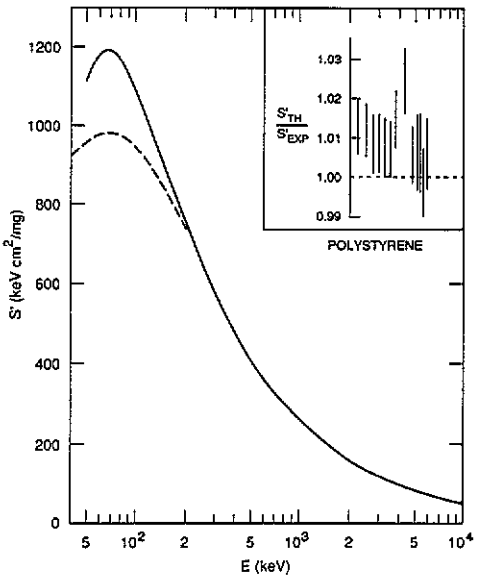

Figure 12. Stopping power of polystyrene for protons from the optical-data model (full curve) compared with tabulated values [33]. The inset shows the ratio of theory to experiment [34, 35], including experimental error estimates, for energies from 2 to 6 MeV.

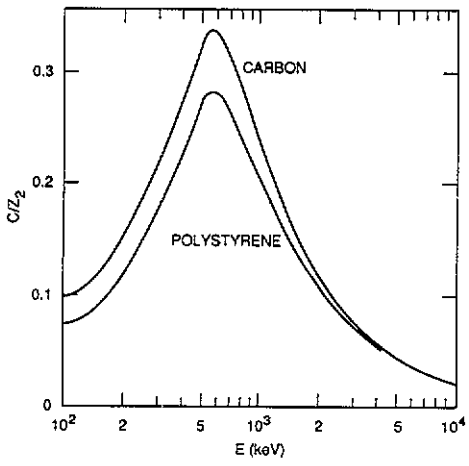

Figure 13. Shell corrections for carbon and polystyrene from the optical-data model.

As an approximate correction, the values of $\mathrm{Im}(-1/\varepsilon)$ for $\hbar\omega \geqslant 1000$ eV (onset of L-shell contributions) were increased by ~8% to give the expected value $\pi\Omega_p^2/2 = 7.194$ au and $I = 326$ eV, a more acceptable result. Mass stopping powers calculated with these modified data are represented by the full line in figure 14. The broken curve is from a fit to a wide range of experimental data [27]. At the lower energies the calculations go from ~27% below the fit curve at 100 keV, to ~6% above it at ~500 keV. For $E > 1$ MeV the two results agree to within 2%. The shell correction for copper extracted from the optical-data model is shown by the full curve in figure 15; the onsets of L- and K-shell electron contributions to L_0 are indicated for reference.

A more detailed comparison is given in table 2. For the lower-energy set of data, left column, differences range from ~4% at 1.2 MeV, 0.6% at 2 MeV, to 1.8% at 2.8 MeV. In the higher-energy range, right side column, our results are less than 3% greater than the Nara data and less than 1.6% greater than the Risö data. Above 12 MeV our calculations agree with both data sets to within 1%. Even with the *ad hoc* modification of the copper optical data, reasonable agreement between the calculations and data is found for $E > 200$ keV.

5. Summary

An optical-data model for evaluation of stopping powers of matter for protons and antiprotons was described and validated for the well-studied case of aluminum. The results and comparisons described for four materials indicate the model should work well overall for energies $\geqslant 100$ keV when sufficient optical data are available; L_0 for

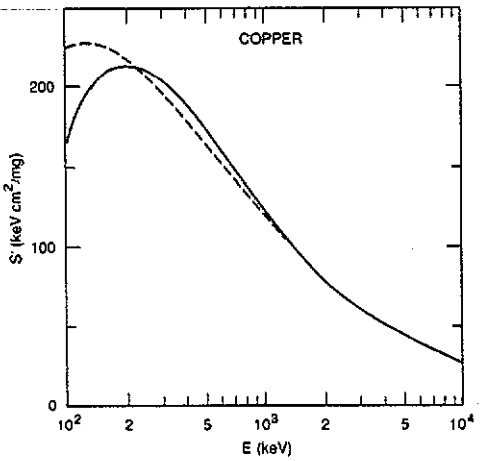

Figure 14. Stopping power of copper for protons from the optical-data model, full curve, compared with a fit to experimental data [27].

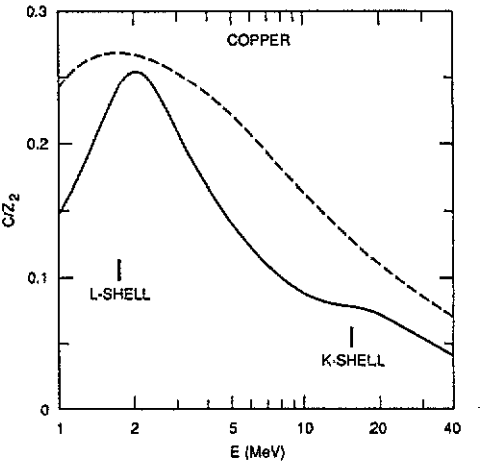

Figure 15. Shell-correction term for copper from the optical-data model, full curve, compared with recommended form [30]. The labelled marks show the energies at which the L-shell and K-shell electrons begin to contribute to L_0.

Table 2. Stopping power of copper for protons (in keV cm^2 mg^{-1}).

E (MeV)	This work	Aarhus [22]	E (MeV)	This work	Nara† [16]	Risö [28]
1.2	111.0	106.0	3	62.74	61.27	62.43
1.4	100.8	97.69	4	52.31	50.87	51.65
1.6	92.39	90.46	5	45.09	43.84	44.40
1.8	85.39	84.41	6	39.76	38.70	39.14
2.0	79.78	79.29	7	35.65	34.78	35.11
2.2	75.39	74.80	8	32.38	31.66	31.91
2.4	71.57	70.87	9	29.72	29.10	29.32
2.6	68.35	67.38	10	27.49	(27.15)	26.98
2.8	65.41	64.28	12	23.99	(23.63)	23.76

† Table 6, 'smoothed data'

protons up to 10 MeV requires optical data up to 5440 eV. While comparisons of the model predictions with very accurate experimental data are quite reasonable, it might be useful to explore the origins of remaining, small, systematic differences. The effective charge of the proton was assumed to be equal to one, in accord with current assessments [37]. The minimum impact parameter for calculating L_1 was chosen principally for pragmatic reasons; clearly, more theoretical study of the Barkas-effect correction is needed.

A nice feature of the optical-data model is that shell corrections are included automatically while in Bethe theory they must be provided by separate calculations. Shell corrections extracted from the model showed reasonably good agreement with other information.

Acknowledgments

This material is based on work supported by the National Science Foundation under Grant No. INT-8716311, and the Office of Health and Environment Research, US

Department of Energy, under contract DE-AC05-84OR21400 with Martin Marietta Energy Systems, Inc. The US government has certain rights in this material.

References

[1] Inokuti M 1971 *Rev. Mod. Phys.* **43** 297
[2] Inokuti M, Itikawa Y and Turner J E 1978 *Rev. Mod. Phys.* **50** 23
[3] Ashley J C 1988 *J. Electron Spectrosc. Relat. Phenom.* **46** 199
[4] Ashley J C 1990 *J. Electron Spectrosc. Relat. Phenom.* **50** 323
[5] Arakawa E T, Dolfini S M, Ashley J C and Williams M W 1985 *Phys. Rev.* B **31** 8097
[6] Ahlen S P 1980 *Rev. Mod. Phys.* **52** 121
[7] Lindhard J 1954 *K. Dan. Vidensk. Selsk., Mat.-Fys. Medd.* **28** 1
[8] Ritchie R H 1959 *Phys. Rev.* **114** 644
[9] Fano U 1963 *Ann. Rev. Nucl. Sci.* **13** 1
[10] Ashley J C, Ritchie R H and Brandt W 1972 *Phys. Rev.* B **5** 2393
[11] Bloch F 1933 *Ann. Phys., Lpz.* **16** 285
[12] Bichsel H and Porter L E 1982 *Phys. Rev.* A **25** 2499
[13] Ashley J C, Anderson V E, Ritchie R H and Brandt W 1972 Z_1^3-effect in the stopping power of matter for charged particles: tables of functions *National Auxiliary Publications Service* (*NAPS*) *Document No 02195*
[14] Maynard G and Deutsch C 1982 *J. Physique* **43** L223
[15] Bichsel Hans 1990 *Phys. Rev.* A **41** 3642
[16] Ishiwari R, Shiomi-Tsuda N and Sakamoto N 1988 *Nucl. Instrum. Methods* B **35** 118
[17] Ishiwari R, Shiomi-Tsuda N and Sakamoto N 1988 *Nucl. Instrum. Methods* B **31** 503
[18] Shiles E, Sasaki T, Inokuti M and Smith D Y 1980 *Phys. Rev.* B **22** 1612
[19] Smith D Y, Shiles E and Inokuti M 1983 *Argonne Nat. Lab. Rep.* ANL-83-24
[20] Jackson J D and McCarthy R L 1972 *Phys. Rev.* B **6** 4131
[21] Lindhard J 1976 *Nucl. Instrum. Methods* **132** 1
[22] Andersen H H, Bak J F, Knudsen H and Nielsen B R 1977 *Phys. Rev.* A **16** 1929
[23] Ishiwari R, Shiomi N and Sakamoto N 1982 *Nucl. Instrum. Methods* **194** 61
[24] Gabrielse G, Fei X, Orozco L A, Rolston S L, Tjoelker R L, Trainor T A, Haas J, Kalinowsky H and Kells W 1989 *Phys. Rev.* A **40** 481
[25] Direct evaluation of L_1 for *silicon* using p and $\bar{p}$ energy loss in thin targets for energies of 500 keV to 3 MeV were made by
Andersen L H, Hvelplund P, Knudsen H, Møller S P, Pedersen J O P, Uggerhøj E, Elsener K and Morenzoni E 1989 *Phys. Rev. Lett.* **62** 1731
Evaluation of L_1 using optical data for silicon produced values within 3% of those for aluminum in this energy range for $a = 1/1.781v$. These theoretical values differ by less than 15% from (above) the broken line in figure 4 of the reference cited above and thus are in reasonably good agreement with the experimental data.
[26] Bethe H A and Ashkin J 1953 Passage of radiations through matter *Experimental Nuclear Physics* vol. 1, ed E Segre (New York: Wiley) p 166
[27] Andersen H H and Ziegler J F 1977 *Hydrogen Stopping Powers and Ranges in All Elements* (New York: Pergamon)
[28] Sørensen H and Andersen H H 1973 *Phys. Rev.* B **8** 1854
[29] Bonderup E 1967 *K. Dan. Vidensk. Selsk., Mat.-Fys. Medd.* **35** 1
[30] 1984 Stopping powers for electrons and positrons *International Commission on Radiation Units and Measurements* (*ICRU*) *Report 37* (Bethesda, MD 20814) p 12
[31] Inagaki T, Arakawa E T, Hamm R N and Williams M W 1977 *Phys. Rev.* B **15** 3243
[32] Ashley J C 1979 *Phys. Rev.* B **19** 5429
[33] Janni J F 1982 *At. Data Nucl. Data Tables* **27** 147
[34] Porter L E, Naylor H and Duder J C 1978 *Nucl. Instrum. Methods* **155** 25
[35] Porter L E 1980 *Phys. Rev.* B **22** 2221
[36] Hagemann H-J, Gudat W and Kunz C 1974 *Deutsches Elektronen-Synchrotron Report* DESY SR-74/7 (Hamburg) 1975 *J. Opt. Soc. Am.* **65** 742
[37] Ziegler J F, Biersack J P and Littmark U 1985 *The Stopping and Range of Ions in Solids* (New York: Pergamon)